Solid-Binding Proteins – Bridging Synthesis, Assembly and Function in Hybrid and Hierarchical Materials Fabrication

Karthik Pushpavanam[1], Jinrong Ma[2], Yifeng Cai[1], Nada Y. Naser[1], and François Baneyx[1,2]*

Department of Chemical Engineering[1], and Molecular Engineering and Sciences Institute[2], University of Washington, Box 351750, Seattle, WA, United States

*email: baneyx@uw.edu

Keywords Solid-binding peptides; Materials-binding peptides; Solid-binding proteins; Protein Engineering; Bionanotechnology; Biological nanotechnology

Abstract

There is considerable interest in the development of hybrid organic-inorganic materials because of the potential for harvesting the unique capabilities that each system has to offer. Proteins are an especially attractive organic component due to the high amount of chemical information encoded in their amino acid sequence, their amenability to (re)design, and the many structures and functions they specify. Compared to poorly controlled physico-chemical processes, genetic installation of solid-binding peptides (SBPs) within protein frameworks affords control over positioning and orientation, and a path towards controlled synthesis and precise assembly of functional materials and devices, all while harnessing the built-in properties of the host scaffold. Here, we review the current understanding of the mechanisms through which SBPs bind to technologically relevant interfaces with an emphasis on the variables that influence the process, and highlight the last decade of progress in the use of solid-binding proteins for hybrid and hierarchical materials synthesis.

1. INTRODUCTION

There is a long list of desirable attributes for next generation materials. Ideally, their structure would be user-specified and optimized for a particular function, they would be self-healing and reconfigurable, and they would be produced by environmentally friendly and inexpensive means. Materials with such properties have been generated by biological systems over the course of 3.5 billion years of evolution, with an objective function imposed by the need for survival and success in an ecological niche. Considering the diversity of materials found in nature, the long-standing interest of scientists and engineers in understanding and exploiting biological principles and bioinspired approaches for the design of novel materials is not surprising. However, controlling the synthesis, assembly and integration of these materials with the exquisite precision of biological systems remains a formidable challenge.

Consider, for example, the use of self-assembled organic templates to orchestrate the growth of inorganic materials that mimic biomineralized structures (1). Templates ranging in size from the nano- to the microscale, and in composition from nucleic acids to polymers have been used for this purpose. However, all exhibit shortcomings. DNA nanotechnology, which relies on programmable Watson-Crick base pairing to yield deterministic structures at the nanoscale, was harnessed to fabricate nanosized tetrahedral and cubic architectures that were in turn used as templates to control the growth of amorphous silica onto the surface of the DNA framework (2). However, loss of template structural integrity due to incomplete binding of stabilizing Mg^{2+} ions

during mineralization likely results in inconsistent production of structurally similar DNA-inorganic hybrids (3). On the other end of the size and composition spectrum, self-assembling phospholipids, the building blocks of cell membranes, were used to fabricate lipid nanoparticles that self-assembled into larger microstructures, and the resulting species were exploited as reaction vessels for silicification reactions (4). Unfortunately, the lipid nanoparticles aggregated into a broad range of non-uniform microstructures, impeding the synthesis of uniform silica particles (5). An emerging middle ground are peptoids, a class of sequence-defined peptidomimetic polymers that can be designed for self-assembly into a variety of nanostructures, some of which have been used to template the growth of inorganic materials (6). Peptoids have the advantage of enhanced stability and simple and inexpensive at-scale synthesis. However, the lack of backbone hydrogen bonding diminishes the ability to form β-sheets, a critical component in the assembly of certain higher order structures (7). In short, although template-based approaches have improved our understanding of biomimetic material synthesis and allowed for greater precision in dictating material properties, they remain far from outperforming the protein- and peptide-based schemes used by sea urchins to fabricate calcite spicules, mollusks to grow nacre shells, and humans to produce teeth and bone.

Proteins and peptides offer a promising route for the bottom-up synthesis and assembly of materials, systems and devices because of their small size (typically a few nanometers) and the chemical and structural versatility made possible by 20 natural amino acids and many more unnatural ones (there are 20^6 or 1.28 billion possible combinations of natural heptapeptide sequences!) (8). Furthermore, from self-assembly to ligand-binding, and from molecular transport to catalysis, the broad range of functions that proteins specify can be incorporated within target

materials or even specified from scratch using computational protein design (9). A number of excellent reviews have described how proteins have been exploited in the development of novel materials for bioelectronics, regenerative medicine and catalysis (10-12). Here, we focus on recent progress in the understanding of the mechanisms that underpin peptide-solid recognition, and on the use of genetic and computational engineering to enable the design of solid-binding proteins that will make the next generation of hierarchical and hybrid materials possible.

2. SOLID BINDING PEPTIDES

Living systems have evolved a variety of approaches to survive and thrive in adverse environments. One of the most successful involves envelopment within inorganic layers formed when peptides, proteins, or other biomacromolecules interact with precursor ions (13). Because the natural inventory of biomineralizing peptides and proteins, and the number of inorganic phases they precipitate are both limited, alternative approaches have been developed to identify solid-binding peptides (SBPs) capable of binding, organizing, precipitating, reducing or controlling the phase or morphology of a broad range of materials.

Since the seminal identification of gold-binding peptides by Stanley Brown (14), it has been recognized that combinatorial display technologies can be used to identify short peptides that bind to target inorganic or synthetic surfaces through noncovalent interactions and without a need for additional post-chemical modification and/or physical processing. The mainstay approach for isolating new SBPs involves the use of M13 filamentous bacteriophage display. In the M13 Ph.D.™ system commercialized by New England Biolabs, random heptamers or dodecamers are expressed as linear or disulfide-constrained fusions to the phage's pIII minor coat protein, resulting

in their pentavalent display in the library of virions (15). Another popular technology, the FliTrx™ system, relies on multivalent display of disulfide-constrained libraries of dodecapeptides on defective *E. coli* flagella as Thioredoxin 1 (TrxA) active site loop inserts installed within the FLiC major flagellar protein. Unfortunately, the FliTrx system is no longer commercially available.

The probability of identifying a peptide capable of high-affinity binding to a target solid is dictated by library size and diversity, the ease with which a particular sequence is expressed on the displaying organism's surface, and the efficiency of phage (or cell) amplification. Compared to bacteriophage and flagellar display libraries which contain 10^6 to 10^9 unique variants, mRNA and ribosomal display platforms allow for larger library size (10^{12} to 10^{14} variants) as they are not limited by transformation efficiency and organismal display (16, 17). Ribosomal display harnesses the production of stable, ribosome-bound peptide-mRNA complexes from a source DNA library. The protruding peptide segment of the ribosomal complexes is used for target recognition while the linked mRNA connects phenotype to genotype. The disadvantages of the approach include nonspecific binding of ribosomal particles to the target material and inefficient display due to peptide-ribosome interactions. These limitations can be addressed by using mRNA display in which peptide-mRNA complexes are formed through a covalent linkage with puromycin. However, concerns with mRNA stability and purification challenges have limited the use of the platform. It should also be noted that while large libraries are conceptually desirable, the use of ribosomal and mRNA display for SBP identification has remained largely untapped because organismal display technologies often provide more candidates that can be thoroughly characterized with low throughput techniques.

In typical biopanning workflows, the library of organisms is contacted with a well-characterized target solid, binders are amplified (phages) or cultivated (cells) and the enrichment cycle is repeated 3 to 5 times. The library may be first contacted with a non-target material to remove confounding or undesirable binders (e.g., when SBPs specific for a particular crystal facet are needed), and the stringency of elution conditions may be increased to select higher affinity binders (18, 19). In phage display, Sanger sequencing is used at the completion of each biopanning step to decode the sequence of randomly picked peptides recovered from the display pool and to monitor their enrichment. While this workflow is widely used, it can be inefficient, suffer from phage amplification bias, and miss potentially useful binders if the surface is highly heterogeneous. Next-generation sequencing (NGS) was recently found to have promise in addressing these shortcomings (20). In a selection of polypropylene-binding peptides, Börner and coworkers found that NGS of the entire SBP pool after a single round of biopanning yielded some of the same sequences found by Sanger sequencing after three rounds of biopanning, along with a number of high-affinity sequences that were missed in the traditional workflow. In addition, statistical analysis of NGS datasets provided an early view of amino acid enrichment and suppression, as well as positional information on enriched residues. Such information could prove very useful for rational SBP design.

3. MECHANISM OF BINDING

The binding of SBPs to surfaces is mediated by a spectrum of non-covalent interactions that result in macroscopic dissociation constants ranging from the micro- to sub-nanomolar range. There are however three classes of parameters to consider when examining the nature of binding: (1) the sequence, conformation and self-association propensity of the SBP; (2) the curvature, chemistry,

topography and crystallography of the target surface; and (3) the solutions conditions, with pH, ionic strength, and ion identity being most important. We refer readers interested in the experimental tools used to investigate SBP binding to an excellent review by Bansal et *al.* (21). Below, we discuss seminal and recent studies that daylight the role of sequence, structure, interface and solution conditions in the binding of SBPs to inorganic surfaces with a focus on technologically relevant two-dimensional (2D) materials (graphene), noble metals (gold and silver) and metal oxides (silica and titania).

3. 1. Binding to Graphene

Since the discovery of graphene in 2004, 2D materials have attracted significant attention due to their unique mechanical, optical and electrical properties and there has been growing interest in isolating peptides binding to these substrates for sensing, medical and opto-electronic applications (22). Sarikaya and colleagues isolated the GrBP5 graphite-binding peptide (**IMV**TESSD**YSSY**) and found that it was capable of self-organizing into ordered structures over micrometer length scales on highly oriented pyrolytic graphite (HOPG) (23). Substituting phenylalanine (F) or tryptophan (W) for the C-terminal tyrosines (Y) reduced HOPG binding affinity, while changing the N-terminal "IMV" sequence to "TQS" led to a porous and disordered surface arrangement. These findings were taken to underscore the need for an amphiphilic character to mediate the combination of surface and intermolecular interactions conducive to long-range ordering. Katoch *et al*. found that peptide GAMHLP**W**HMGTL adopts a helical structure and forms a continuous open mesh layer on HOPG (24). The authors used molecular dynamics (MD) simulations to probe the significance of the central tryptophan in graphene binding. They found that replacing this residue by an alanine (A) led to a significant decrease in interaction energy by distorting the

tryptophan-promoted helical conformation thought to be critical for orienting the peptide parallel to the graphene surface.

Hughes *et. al* also employed MD to show that the P1 peptide (HSS**YW**YA**F**N**N**KT) is stabilized in a helical conformation on the surface of graphene through π-π interactions involving the side chains of Y4, W5, F8 and N9 (25). Indeed, when two of these so-called anchor residues (Y4 and W5) were replaced by alanine, the resulting P1A3 peptide formed extended structures and there was a concomitant decrease in π-π interactions at the graphene surface. Yet, the authors also observed enhanced contact between amino acids vicinal to the substitution sites and surfaces, illustrating the relevance of the surrounding sequence and conformation in graphene binding. In the case of MSI-78(C1) (CGIG**KF**L**KK**A**KKF**G**K**A**F**A**K**QL**KK**), a balanced distribution of hydrophilic lysine (K) and phenylalanine anchor residues caused the α-helical peptide to lie down on graphene (26). Altering the distribution by converting F13 and F17 to alanine produced a peptide with two segments, one exhibiting a parallel and the other a perpendicular orientation to the graphene surface. Using principles derived from this study, the same group redesigned the antibody-binding GB1 domain of *Streptococcus* Protein G so that it would bind to graphene without undergoing surface-induced denaturation (27).

Much less information is available on how SBPs bind to other 2D materials including molybdenum disulfide (MOS_2) and hexagonal boron nitride (hBN). However, recent work exploring similarities and differences in the binding of SBPs to various families of 2D materials has yielded new insights that might prove useful to design selective binders for the development of bio-opto-electronic devices (28, 29).

3.2. Binding to Gold

Because of their unique surface plasmon properties and inert nature, gold surfaces have been extensively investigated. One of the most commonly employed gold-binding peptide, l-AuBP2 (WALRRSIRRQSY), exhibits an extended helical polyproline type II (PPII) conformation and exhibits a free energy of adsorption (ΔG_{ads}) on gold of approximately -9.0 kcal/mol (30). Conversion of the peptide from a linear to a cyclic form by formation of a disulfide bridge between flanking cysteine (C) residues interfered with the formation of the PPII structure and led to a random conformation that increased gold binding affinity. In addition, repeating the sequence of a different gold binder called l-GBP1 (MHGKTQATSGTIQS) three times increased ΔH_{ads} by 5 times indicating stronger binding propensities accompanied by an entropic gain associated with the displacement of water molecules by a more conformationally flexible peptide (31, 32). Interestingly, a further increase in the number of tandem repeats to 9 and 11 caused a decrease in binding affinity, suggesting the need for balance between conformational flexibility and stability (33).

How surface crystallography impacts binding was investigated using l-AuBP1 (WAGAKRLVLRRE), an SBP that displays higher affinity for Au(111) relative to Au(100) (34). MD simulations revealed that binding to Au(111) is mediated by 10 of the peptide's 12 residues, but that only 4 amino acids make contact with a reconstructed Au(100)-(1x1) surface. In addition, adsorption of the peptide to an Au(100) surface expelled on average 5 ± 8 water molecules compared to 35 ± 10 waters for Au(111), suggesting an indirect binding mechanism regulated by the strength of the interfacial hydration layer. Pd4 (TSNAV**H**PTLR**H**L), an SBP originally selected for its ability to bind palladium was used to probe the role of histidine (H) residues in gold binding (35, 36). Single H6A and H11A substitutions resulted in ~2-15% lower binding affinities,

indicating that single amino acid changes can have substantial effects. However, and counter-intuitively, combining the two substitutions led to a peptide whose affinity for gold was identical to that of wild type Pd4. Although MD simulations did not reveal the presence of obvious anchor residues in Pd4, a segment extending from N3 to P7 was found critical in determining binding affinity to gold. In addition, the time that the NAV triad spent in contact with the surface was significantly higher for Pd4-3 (TSNAV**A**PTLR**A**L) than for the wild type, highlighting the importance of local characteristics in surface binding. Finally, an interesting study highlighted the effect of surface topography on the adsorption of A3 (AYSSGAPPMPPF) to Au(111) (37). The presence of high surface energy regions in the form of grain boundaries and step edges allowed for a higher conformational stability of the peptide, resulting in an increased binding affinity relative to a pristine Au(111) surface.

3.3. Binding to Silver

Silver is another plasmonic material that has the added benefit of exhibiting antibacterial properties. Peptides AgBP1 (TGIFKSARAMRN) and AgBP2 (EQLGVRKELRGV) have been found to adsorb to Ag(111) surfaces through a mix of direct interactions and interfacial hydration layer mediated binding (38). Although they have rather high adsorption energies on silver (between -8 and -9 kcal/mol), MD simulations indicate that the two SBPs only form a small number of long-lasting contacts with the surface. Moreover, while AgBP1 uses sequential residues (S6 to N12) as anchors, AgBP2 relies on more distal amino acids (Q2, G4, R6 and G11) to achieve binding, highlighting the challenge in categorizing the binding of peptides based on the sum of the amino acids binding affinity towards a surface. Interestingly, although the two peptides were selected on silver, they have a similar affinity for Au(111) surfaces, possibly mediated through a direct interaction with the metal surface, while the water-mediated interactions drives peptide

adsorption onto silver. As far as individual amino acids are concerned, a role for arginine was indirectly demonstrated when the central phenylalanine of the silver-binding SL**F**RS peptide was replaced by lysine (39). Removal of the bulky F3 favored contact of R4 with the Ag(111) surface, simultaneously increasing interfacial peptide stability. A separate study confirmed that the guanidinium moiety of arginine in peptide M**R**KDV is responsible for orienting the molecule on the Ag surface (40).

3. 4. Binding to Silica

Silica (SiO_2) is an inexpensive and earth-abundant material that has garnered interest in application spaces ranging from catalysis to biomedicine. Although numerous silica-binding peptides have been isolated, they are compositionally diverse and exhibit little sequence homology. This is in part due to the fact that, in addition to composition and conformation, peptide concentration, surface curvature and surface chemistry all have a profound influence on silica binding. A series of articles by Perry and coworkers nicely illustrate the importance of these factors. Several laboratories have reported that the basic side chains of lysine and arginine (R) play an important role in mediating the binding of SBPs to SiO_2 by engaging with negatively charged surface siloxide groups ($\equiv SiO^{-}\ldots Na^{+}$) on the silica surface. The cationic peptides pep1 (**KSLSR**HDHIHHH), pep4 (MH**RS**D**L**M**S**AAV**R**), Si4-1 (M**S**PHPHP**R**HHHT) and Si4-10 (**R**G**RRRRLS**C**RLL**) isolated by the Perry laboratory are no exception as they efficiently adsorb at < 0.2 mg/ml (a concentration considered low for a synthetic SBP) to ~80 nm amorphous silica nanoparticles (41). However, while the anionic peptide 7-mer (LDHSLHS) exhibits minimal binding under the same conditions, increasing its concentration above ~1 mg/ml results in adhesion, a result that emphasizes the importance of concentration effects and suggests that caution should be exerted

when categorizing SBPs as “strong” or “weak” binders. Perry and coworkers also found that hydrophobic interactions can mediate silica binding by showing that whereas both the neutral peptide S2 (AFILPTG) and the cationic peptide S1 (KLPGWSG) bind to ~80 nm heat-treated silica nanoparticles devoid of surface silanols, S1 exhibits a remarkable decrease in affinity relative to S2, likely because the decreased hydration layer favors short-range hydrophobic interactions that are important for the binding of the latter peptide (42). The team highlighted the role of conformational flexibility by demonstrating that whereas a H6A mutant of pep1 exhibits high affinity for silica due to the increased degrees of freedom associated with the removal of the bulky central histidine, a H11A variant has lower affinity for the material because a more rigid backbone leads to reduction in the number of contacts with the surface (41). To probe the influence of surface curvature/area, Puddu *et al.* studied the interaction of S1, S2 and 7mer with nanoparticles ranging in size from 28 to 500 nm and found that binding affinity decreased with size irrespective of the SPB’s charge or pI (43). Finally, the influence of surface chemistry was explored using nanoparticles functionalized with amino or methyl groups: charged SBPs had high affinity for surfaces carrying complementary charge, while the neutral S2 peptide had high affinity for methylated surfaces due to enhanced interaction of aliphatic and aromatic side chains with the methyl groups on the silica surface. Although these results were not surprising, further work demonstrated the importance of the degree of functionalization (44). For instance, the 7mer peptide interacted less efficiently with a surface functionalized with a high density of amino groups compared to one that had low levels of functionalization, indicating that binding depends less on overall charge and more on the local characteristics of the histidine residues.

Using Car9 (DSARGFKKPGKR) fused to superfolder green fluorescent protein (sfGFP), we have found that peptide self-association can have a profound effect on the modality of silica adhesion.

The high-affinity interaction of Car9 with silica is mediated by a spectrum of persistent interactions between the positively charged side chains of lysine and arginine and the negatively charged SiO_2 surface. As surface coverage increases, Car9 peptides associate with one other at the interface to form higher order oligomers. This cooperative adhesion phenomenon gives rise to high-affinity binding and a distinct sigmoidal sensorgram in SPR experiments (45, 46). While mutations that disrupt the compactness of the peptide (e.g., F6A and P9A-G10A) lead to a slight decrease in the free energy of binding, the process remains cooperative. In sharp contrast, conversion of anchor basic residues to alanine or glutamine (Q), reduces surface coverage and severely curtails peptide self-association, leading to a traditional Langmuir adhesion behavior in SPR experiments. Remarkably, there only was an about 20% reduction in free energy of adsorption between theses mutants and the wild type (from ~ -12.5 to ~ -10 kcal/mol), indicating that a rich range of kinetic behaviors exist in a narrow energetic band.

3.5. Binding to Titania

Titanium dioxide (titania; TiO_2) is a wide bandgap semiconductor that has found use in applications ranging from water splitting to photocatalysis. Choe and colleagues isolated a disulfide-constrained titania-peptide called STB1 (CHKKPSKSC) and compared its TiO_2-binding affinity to that of LSTB1, its linear counterpart (AHKKPSKSA) (47). The higher conformational flexibility of unconstrained LSTB1 allowed for a broader range of sidechain orientations and more effective electrostatic interactions with the TiO_2 surface, resulting in increased binding affinity relative to STB1. Remarkably, the constrained peptide had a higher selectivity towards SiO_2 while LSTB1 exhibited a similar propensity to bind to either oxide.

Ti-1 (QPYLFATDSLIK) and Ti-2 (GHTHYHAVRTQT), which have similar overall charge but different amphiphilic characteristics -- Ti-1 displays a slightly more hydrophobic character than Ti-2 -- were isolated as high-affinity titania binders by Sultan *et al.* (48). These subtle differences led to two distinct modes of binding with Ti-1 using a larger number of residues to make shorter-lived contacts with the interface, and Ti-2 using a smaller number of anchor residues along the sequence to make long-lasting contacts with the interface.

Peptide Ti-12-3-1 (RKLPDAPGMHTW) was one of the first titania-binding peptides described in the literature and remains one of the most extensively characterized. Using an alanine scan, Sano *et al.* found that the hexameric sequence RKLPDA was responsible for binding in a process involving arginine and aspartic acid residues (the MRKLPDA peptide which also binds to silica later became known as mTBP). They postulated that the two oppositely charged side chains interacted with $Ti\text{-}O^-$ and $Ti\text{-}OH_2^+$ regions on the titania surface (49). Subsequent saturation transfer difference NMR experiments conducted at pH 7 revealed that binding predominantly involved contacts between the positive side chains of arginine and lysine with $Ti\text{-}O^-$ surface groups, suggesting an important role of hydrogen ions in determining peptide binding affinity (50). The recognition of interfacial water layer by charged anchor residues (R and D or K and D) was later found to be critical in determining binding affinity to the titania surface (51). Indeed, replacement of D5 by alanine caused detachment of the peptide from the water layer, likely due to decreased interaction of the carboxylate group of aspartic acid (D) with hydrogen atoms projecting outwards from the interfacial water layer. In addition to electrostatics, the loss of peptide flexibility associated with a P4A mutation caused peptide detachment and lower titania binding affinity compared to the wild type (51). A separate study simulating the binding of the RGD trimer to the TiO_2(110) surface in the presence of monovalent (Na^+, K^+ and Rb^+) and divalent (Sr^{2+}, Ca^{2+} and

Mg^{2+}) ions further showed that cations influence binding by modulating the hydration layer, and that significant differences in binding affinity arise in the presence of divalent cations relative to monovalent cations (52).

4. DESIGNER PROTEINS

The creation of designer proteins that tailor, improve or exceed the functions and activities of natural proteins remain a frontier of biological research that continue to motivate and challenge scientists and engineers. Although progress in our understanding of structure-function relationship (53, 54) has fueled considerable advances in the design of multi-functional chimera (55), and despite new frontiers opened by computational protein design (56), the promise of these biomacromolecules has not been fully realized (57). Of particular interest is realizing symbiosis between organic and inorganic components to create synergies between what are traditionally considered divergent classes of materials. This has been possible by incorporating SBPs within genetically engineered or computationally designed protein frameworks to create a new class of polypeptides that we call solid-binding proteins. These powerful tools have found applications ranging from regulating and controlling crystal growth and polymorphism, to promoting enhancements in structural, binding and catalytic properties. Below, we describe a selection of recent efforts that have aimed at creating organic-inorganic hybrid materials that harness the best of both worlds using solid-binding proteins (**Figure 1**).

4.1. Intrinsically Disordered Proteins

While the biological function of a protein is typically viewed as being specified by its 3-dimensional conformation, it is now clear that intrinsically disordered proteins (IDPs), whose

function is independent form structure, exist in all organisms (58). IDPs are characterized by a lack of order-promoting residues (Y, W and F), and an enrichment in disorder-promoting residues (K, P and S). Despite - or because of - their inability to fold into unique structures, IDPs exhibit spatiotemporal structural heterogeneity, adaptability to environmental perturbations, and extraordinary structural conformations.

Elastomeric proteins are present in the skin and ligaments of many organisms, providing toughness and elasticity for maintenance of physiological function. Elastin-like polypeptides (ELPs) are recombinant polypeptides with the repetitive amino acid sequence $(VPGXG)_n$ where X represents any amino acid except proline and *n* is the number of repeats. ELPs exhibit a reversible, thermoresponsive phase transition that is sequence-dependent (59). By appending the R5 silica-binding peptide (SSKKSGSYSGSKGSKRRIL) to the hydrophilic terminus of a diblock copolymer containing hydrophilic and hydrophobic ELP segments, and by exploiting its temperature-dependent self-assembly into spherical micelles displaying multiple R5 copies on their coronae, Lopez and coworkers were able to control the size of silica nanoparticles precipitated from phosphate-free silicic acid solutions (60). Micelles made with ELP-R5 led to the production of hybrid particles of uniform size (~50 nm), while neither control micelles lacking the R5 peptide, nor unassembled ELP-R5 promoted nanoparticle formation. These results suggested that silicification is directed by an increase in the density of positive charges originating from the lysine and arginine side chains of multiple R5 peptides that become spatially colocalized during micellization. To better understand the process, the same group undertook an in-depth study of the role of the R5 extension and ELP micellization on silica adsorption (61). Fusing R5 to ELP increased the adsorption rate of the unimer and led to greater silica surface coverage relative to unmodified ELP. Furthermore, ELP-R5 micelles were tightly packed and evenly dispersed on

silica surfaces, while adsorption of the parent ELP micelles led to "patchy" coverage. Unfortunately, ELP-R5 micelles immobilized on silica surfaces were no longer thermally responsive, while the un-micellized unimers retained their temperature responsive property. These observations may help design smart surfaces through the incorporation of SBPs on ELPs to control structure–architecture–function relationship.

Silk proteins derived from spiders exhibit remarkable elastic behaviors and their mechanical properties by weight are far superior to those of silkworm silk. Unfortunately, farming spiders for large scale silk production is difficult due to their venomous and predatory nature. Silk-like polypeptides, which combine structural motifs native to spider silk proteins with a GPGXX/GPGGX elastic motif and with strength motifs composed of repeated (GA) or (GGX) sequences, are an attractive recombinant alternative to native silk proteins (62). Kaplan and Perry fused the R5 peptide to the N- or C-terminus of such a protein – a 15-mer repeat of the 33 amino acid sequence SGRGGLGGQG AGAAAAAGGA GQGGYGGLGSQGT – to investigate the influence of SBP location on silicification (63). While both proteins promoted silica precipitation, the diameter of the particles obtained with the C-terminal fusion (~300 nm) was half that produced by the N-terminal fusion. The formation of discrete particles was attributed to the self-association of the R5 peptide leading to the formation of "protein droplets/aggregates" within which silicification proceeded. In a separate study, the Ag4 silver-binding peptide (NPSSLFRYLPSD) was fused to a 6-mer and a 15-mer repeat of the spider silk domain to synthesize antibacterial coatings in which Ag4-mineralized silver nanoparticles provided microbial killing function and the silk segment enabled processing into films (64). The Ag4-modified 6-mer promoted the formation of ~30 nm homogeneous nanoparticles, while its fusion to the C-terminus of the 15-mer

led to the formation of rod-like morphologies (~60 nm in diameter and ~200 nm in length) which appeared to result from longitudinal aggregation of spherical particles.

Aside from these recent forays, the potential of solid-binding IDPs for the synthesis of hybrid and hierarchical materials remains largely unexplored. Combining a growing arsenal of IDPs and validated SBPs should prove valuable for the development of materials and devices with superior physicochemical properties.

4. 2. Enzymes

Industrial enzymes are playing an increasingly important role in the manufacturing of high value-added chemicals such as fragrances and pharmaceuticals. As a consequence, there has been renewed interest in the development of enzyme immobilization strategies that enhance the stability, enable the reusability, and allow for the facile separation of biocatalysts from sought-after products. Beyond the traditional approaches of physical adsorption, covalent coupling and entrapment, genetic installation of SBPs within permissive sites – locations that accommodate extraneous stretches of amino acids without measurable impact on folding or function – offer a route for enzyme immobilization on non-standard substrates while providing ancillary benefits.

One such advantage is an increase in the yields of overexpressed or aggregation-prone proteins as charged SBPs tend to improve protein solubility. Such an outcome was recently highlighted in a study in which the R5 silica-binding peptide was fused to the difficult-to-express enzymes monomeric sarcosine oxidase (mSOx) and horseradish peroxidase (HRP) that were themselves fused to the mCherry fluorescent protein (mCh) for visualization (65). The 6His-R5-mCherry-HRP fusion was readily isolated from soluble cell fraction, exhibited a Michaelis-Menten constant

(K_m) comparable to conventional HRP isoenzyme mixtures, and, when immobilized on silica, displayed no significant loss in activity over 2 months of room temperature storage while the free protein lost > 80% of its activity. SBPs can also mitigate surface-mediated enzyme unfolding and the associated loss of activity. For instance, when Yang *et al.* attempted to build a sensor for the detection of paraoxon, a model organophosphate, by immobilizing organophosphorus hydrolase (OPH) onto gold nanoparticle-modified graphene, the approach met with minimal success due the loss of OPH's secondary structure (66). However, incorporation of the GBP gold binding peptide to construct 6His-GBP-OPH allowed for efficient recognition of graphene-bound gold nanoparticles with minimal structural loss and improved sensor performance.

Carbonic anhydrase, a molecular catalyst in the reduction of carbon dioxide ($CO_2 + H_2O \leftrightarrow HCO_3^- + H^+$) has attracted attention for its potential to aid with carbon capture. However, the reaction proceeds under thermal and chemical conditions that cause protein denaturation (67). By fusing the silica-binding Si-tag (a truncated ribosomal protein L2) to α-type Carbonic Anhydrase (hmCA) Cha and coworkers were able to achieve a 3-fold increase in enzyme loading on silica diatoms and a 10% increase in activity compared to the unmodified enzyme (68). However, a further increase in loading led to decreased overall activity, possibly due to increased steric repulsion between enzymes and associated misfolding. Fusion of the silica-binding peptide EctP1 (SSRSSSHRRHDHHDHRRGS) to bovine carbonic anhydrase (BCA) II also supported stable enzyme immobilization on silica and titania supports (69). In fact, while EctP1 was originally identified as a silica-binding peptide, there was a 50% increase in the amount of bound protein and a 20% increase in enzymatic activity when a BCA-EctP1 fusion was immobilized onto titania compared to silica. Interestingly, while both immobilized enzyme preparations retained over 90%

of their activity at 50°C (compared to 50% for the free protein), titania-bound BCA-EctP1 remained functional over a much broader range of pH (from 2 to 9 compared to from 7 to 9 in the case of silica).

SBPs can also be useful to orient proteins on substrates. For instance, Kacar *et. al* reported that fusion of a penta-repeat of the GBP1 gold-binding peptide (MHGKTQATSGTIQS) to alkaline phosphatase enabled efficient enzyme immobilization on polycrystalline gold and prevented misorientation and aggregation, as judged by non-contact mode AFM (33). Even more exciting is the fact that SBPs can enhance enzyme function by sequestering key ions. Ackerson and colleagues provided a good demonstration of the latter by using the selenium-binding peptide SeBP (LTPHKHHKHLHA) to modulate the catalytic activity of glutathione reductase-like metalloid reductase (GRLMR), an enzyme capable of reducing selenite and selenate to amorphous selenium nanoparticles (70). When fused near the active enzyme site of GRLMR, the basic residues of SeBP concentrated SeO_3^{2-}precursor anions and supported the formation of a stable dispersion of colloidal selenium nanoparticle (diameter < 50 nm) at micromolar protein concentrations. By contrast, supplementing the solution with SeBP and unmodified GRLMR resulted in the formation of polydisperse particles that were prone to aggregation.

It is finally worth pointing out that accessible amino acids in fused SBPs can be used for further crosslinking reactions in order to improve upon native enzyme activity. As an example, the highly accessible lysine and arginine residues of the silica-binding sequence $VKTQATSREEPPRLPSKHRPG)_4VKTQTAS$ fused to thermostable hemicellulases were cross-linked with glutaraldehyde to form cross-linked enzyme aggregates (CLEAs) that

outperformed the free enzyme formulation by resisting inactivation during recycling (71). Additionally, the covalent nature of the crosslinking protected the enzyme from structural distortions caused by heat and allowed multiple reuses under high temperature (80°C) operating conditions.

4.3. Rings and Shells

Nature generally prefers to produce organized structures of proteins through the self-assembly of smaller subunits rather than relying on the thermodynamically unfavorable process of building a single large protein. This is especially true for ring-shaped protein structures that are commonly found in molecular chaperones, cell cycle regulatory proteins, and metal transporters. In general, the inner ring of these oligomers specify high concentrations of binding sites that capture substrate molecules within a central cavity, while their outer rings preclude undesirable species from accessing that location. The well-defined central cavities provide an ideal environment for templating the fabrication of small (<10 nm) nanoparticles, whose bulk synthesis would otherwise require precise control of mixing and temperature. There has been a number of exciting developments since the pioneering work of the Trent (72, 73) and Aida (72, 73) labs with chaperonins, and we summarize recent advances pertaining to solid-binding proteins below.

Peroxiredoxins (Prxs) are a family of antioxidant enzymes that self-assemble into ring structures with pseudo five- or six-fold symmetry. By appending hexahistidine extensions to the N-termini of *Schistosoma mansoni* peroxiredoxin (*Sm*PrxI) protomers which face the ~6 nm internal cavity of the oligomer, Ardini and coworkers devised a metal ion-based strategy to induce ring self-

assembly (74). The team took advantage of the affinity of histidine residues for Ni^{2+}-NTA functionalized gold nanoparticles to stack individual rings into one-dimensional nanotubes (~60 nm in length) that encapsulated a chain of gold nanoparticles (**Figure 2A**). The imposed symmetry during subunit self-assembly created structurally flat and chemically uniform top and bottom surfaces that displayed approximately 100 thiol groups originating from cysteine and methionine residues. These were used to reduce graphene oxide (GO) surfaces and induce the formation of a *Sm*PrxI-GO-*Sm*PrxI sandwich-like structure (75). Additionally, the engineered polyhistidine tails facilitated nanocomposite "doping" with pre-synthesized gold nanoparticles and promoted the *in situ* production of 4 nm palladium nanoparticles from $(NH_4)_2PdCl_4$. Human Peroxiredoxin Ⅲ (*Hs*Prx3), which assembles into toroidal dodecamers, was also engineered with N-terminal hexahistidine extensions, and the resulting protein (*Hs*Prx3-6His) was investigated for its ability to interact with Au(111) surfaces with the goal of assembling surface-tethered supramolecular protein structures (76). *Hs*PrX3-6His formed a stable dodecamer under both acidic (pH 4.0) and basic (pH 8.0) conditions, while the unmodified protein only did so under basic conditions. Furthermore, scanning tunneling microscopy revealed the existence of macromolecular structures ranging in length from 10 to 450 nm and consisting of stacks of 2 to 112 dodecamers. *Hs*Prx3-6His assembly on Au(111) surfaces involved both face-to-face ring association and ring stacking, with low protein concentrations favoring stacking and higher concentrations promoting mixed assemblies.

The homohexameric ring of the Heme carrier protein 1 (Hcp1) has an inner diameter of 4 nm and a propensity to self-assemble into 1D nanotubes 30 to 100 nm in length through ring stacking. In an effort to exploit this behavior to guide the assembly of gold nanoparticles, Schreiber and coworkers constructed a panel of Hcp1 mutants containing cysteine substitutions (77). One variant,

Hcp1_Q54C, with a single cysteine facing the interior of the ring could accommodate 3-5 nm gold particles within its cavity. Two additional cysteine substitutions (G91C and N159C) provided interaction sites in the lower and upper surfaces of the rings that enabled the assembly of 10 nm gold particles into 1D nanotubes. Finally, addition of 40 nm gold nanoparticles to the mixture led to the production of anisotropic structures in which the large gold particles served as nucleation centers for the production of hedgehog-like structures with branching chains of 10 nm particles.

Populus tremula stress-responsive protein (SP1) is a highly stable dodecameric protein that forms a ring with a ~3 nm pore. The N-termini of each subunit faces the inner cavity and can be made to extend to the bulk solvent by incubating the oligomer with 3M guanidine hydrochloride. This property was exploited to control surface adhesion through fusion of the mTBP titania/silica binding peptide (MRKLPDA) to the protein's N-terminus (78). More recently, Bachar et al. appended a hexahistidine tail or the PdBP palladium-binding peptide (SVTQNKY) to the N-terminus of SP1 and demonstrated the production of ~2.7 nm Pd nanoparticles within the protein core using $PdCl_2$ as a precursor and sodium borohydride as a reductant. Pd nanoparticles could also be produced intracellularly when *E. coli* cells overexpressing the same proteins were exposed to $PdCl_2$ overnight and incubated for 3 additional days at 37^{o}C, presumably due to the action of cellular reductants (79).

Ferritins are intracellular iron-storage proteins that are typically composed of 24 subunits arranged into a shell-like structure with an outer diameter 12 nm and an inner diameter of 8 nm (80). In the Fer8 horse liver ferritin, protomer N-termini project towards the inside of the central cavity while their C-termini faces the bulk solution. Taking advantage of this architecture, Zheng and coworkers modified Fer8 with a N-terminal gold-binding peptide (GBP; MHGKTQATSGTIQS) to encapsulate 5 nm gold nanoparticles, and further extended functionality by engineering the mTBP

peptide at the protein's C-terminus to facilitate particle immobilization on silica surfaces (81). In the presence of low concentrations of the detergent Tween 20, the authors observed strong adsorption of TBP-Fer8-GBP while there was minimal surface coverage with control Fer8-GBP. To achieve controlled synthesis of silica nanoparticles, Nguyen and coworkers fused the Kps silica-binding peptide (KPSHHHHHTGAN) to the N-terminus of human heavy-chain ferritin (Fn), and changed the number of SBPs exposed to the inside of the cavity by altering the ratio of Kps-Fn to wild type Fn subunits (82). Increasing the local density of SBPs gave the team the ability to tune the size of the encapsulated silica nanoparticles from 100 to 500 nm due to enhanced silica precipitation and growth at high Kps valency. In a bid to develop a Hg^{2+} detection platform, Wang and coworkers fused the mercury-binding peptide MBP (GMTCAAC) to the N-terminus of human H-chain ferritin (HuHF) and further labeled this extremity (which is exposed on the surface of the ferritin shell) with the FITC fluorescent reporter (**Figure 2B**) (83). The detection scheme took advantage of the selective and dose-dependent ability of Hg^{2+} ions to reverse the quenching of FITC fluorescence by graphene oxide (GO) due to π-π interaction between dye and GO surface.

To date, only a handful of ring- and shell-shaped proteins have been exploited for hybrid materials synthesis, and the genetic engineering focus has been on the inner cavity. With a growing number of natural and *de novo* designed choices available, there is a universe of possibilities for the creation of composite materials and the templating of user-specified shapes and compositions (84).

4.4. Fluorescent Proteins

Fluorescence proteins (FP) have been extensively used as molecular beacons to light up single molecules, living cells and even whole organisms (85). They share the unique ability of developing

a visible chromophore through a sequence of 3 amino acids enclosed in a β-barrel scaffold. Since *Aequorea victoria* green fluorescent protein (GFP) was first isolated, a series of mutants have been engineered. These include enhanced green fluorescent protein (eGFP) and superfolder green fluorescent protein (sfGFP) with improved fluorescence properties, thermostability and resistance to denaturants, color-shifted mutants that emit fluorescence from the 424 nm (blue) to 655nm (red) regions of the spectrum, and many other practically useful variants (e.g., split, environmentally-, time-responsive and photoactivatable mutants) (86-88). This arsenal of variants, together with the facts that most FPs can be expressed at high level in *E. coli* and that they contain internal permissive sites and solvent-accessible N- and C-termini suitable for SBP insertion, make them ideal scaffolds for the construction of fluorescent solid binding proteins (89). These can in turn be used to visualize and quantify adsorption to - and release from -inorganic substrates, assess the extent and efficiency of biomineralization, and design functional hybrid materials that harness the fluorescent properties of the host scaffold.

The usefulness of FPs for visualizing SPB-mediated protein adhesion to patterned surfaces was explored by Tamerler and coworkers using a tripartite fusion protein between *E. coli* maltose-binding protein, GFPuv and the AgBP2C silver-binding peptide (EQLGVRKELRGV) (90). In these experiments, fluorescence microscopy revealed the details of protein patterns that had been microcontact printed on silver surfaces, or obtained by decorating silver nanoparticles photochemically produced on defined domains of a ferroelectric substrate. Solid-binding FPs have also proven helpful for visualizing the site-specific modification of carbon nanotubes. Our group originally identified Car9 (DSARGFKKPGKR) while biopanning for carbon-binding peptides. Along with Car9, we selected Car15 (RTYLPLPWMAAL), a carbon binder with very different amino acid composition for further characterization. Both sequences were installed within the

active site loop of *E. coli* thioredoxin 1 (TrxA) and the affinity of the resulting proteins for *sp*2-hybridized (graphene-like) or *sp*3-hybridized (diamond-like) carbon assessed by SPR, AFM and pull-down experiments. The exercise revealed that whereas Car15 endows TrxA with the ability to selectively bind to *sp*2-hybridized carbon, TrxA::Car9 does not discriminate between the two materials alloforms (91). We exploited this knowledge and the ease of visualization offered by FPs to show that fusion of Car9 or Car15 extensions to the C-termini of sfGFP and mCherry enabled these proteins to solubilize single-walled carbon nanotubes (SWNTs) from their dried state by binding to their hydroxyl/carboxyl-rich ends (Car9 derivatives) or to their graphene-like sidewalls (Car15 derivatives) (**Figure 3A**). By introducing the Ag4 silver/gold-binding peptide (NPSSLFRYLPSD), or more effectively a cysteine residue, within solvent-exposed loops situated on the opposite side of the sfGFP β-barrel from the SBPs, we further showed that it was possible to decorate the ends or the sidewalls of the SWNT with gold nanoparticles using the bifunctional Car9 or Car15 variants of these proteins (92).

Car9 is a promiscuous material binder that also recognizes silica (93, 94). Remarkably, this interaction can be disrupted in the presence of moderately high concentrations of arginine or lysine, offering a path to control not only the adhesion but also the release of solid-binding proteins from the surfaces they bind. We exploited this feature to show that Car9-tagged versions of sfGFP and mCherry could be printed into single or bicontinuous patterns on glass substrates and microscope slides using PDMS (polydimethylsiloxane) stamps, and that the underlying substrates could be regenerated by incubation with 1M lysine (**Figure 3B**) (95). Additionally, when the same proteins self-immobilized within the percolated aqueous network of silica sol-gels produced upon polycondensation of silicic acid, it was possible to control their release to the bulk solution in a

dynamic fashion by successive incubation of the immobilized protein preparation in buffers containing or lacking 1M arginine (**Figure 3C**) (96).

In the biomineralization space, Olmez *et al.* fused the R5 peptide to GFP, YFP and mCherry to produce silica "biodots" of different colors for imaging applications (97). Under well-established synthesis conditions – i.e., when using hydrolyzed TMOS (tetramethylorthosilicate) in pH 8.0 phosphate buffer – the proteins became encapsulated within a continuous silica matrix and the authors found it necessary to operate at reduced TMOS concentration and to remove unreacted precursor by washing to obtain particles in the 100-200 nm range.

The stability of the sfGFP framework over a broad range of pH has proven useful to study how mutations in the Car9 SBP affect titania mineralization outcomes from acidified solutions of TiBALDH, an alkoxide-like conjugate of titanium. At pH 5.0, it became possible to deconvolute the influence of the protein scaffold from that of the SBP, and while most of the precipitated TiO_2 was amorphous, it contained nanocrystalline inclusions whose phase could be tuned from about 80% monoclinic TiO_2(*B*) to about 65% anatase by introducing single and double-mutations in the SBP (**Figure 3D**) (98). The production of monoclinic inclusions by wild type Car9 was attributed to its ability to self-associate in an extended, yet flexible plane that facilitates the formation of edge-sharing bonds between TiO_6 octahedra - and consequently the production of TiO_2(*B*) crystallites - over thermodynamically preferred anatase nanocrystals that are obtained with the R4QR12Q variant.

The fluorescent properties of the scaffold may also be combined with the adhesive and biomineralizing properties of guest SBPs to create functional materials. For instance, fusing the CT43 zinc sulfide-binding peptide (AGDSSGVDSRSV) to the C-terminus of sfGFP allowed for

the biofabrication of protein-capped Mn-doped ZnS nanocrystals that exhibited the emission signatures of the sfGFP chromophore and inorganic fluorophore when excited at 305 nm (99). Insertion of the Car9 sequence within permissive loop 9 of the protein enabled enrichment of these species on silica microparticles which appeared goldenrod under 305 nm illumination but green under 365 nm light. Moreover, functionalization of the protein corona with a chloramphenicol-specific DNA aptamer via click chemistry enabled visual detection of low concentrations of the antibiotic due to the overlap between the absorption band of chloramphenicol and the excitation band of the nanocrystals.

4. 5. Membrane Proteins

Living system needs precise and reliable means to read environmental stimuli, process information, and respond to changes in the most appropriate manner. Membrane proteins (MPs) play a key role in these processes due to their ability to control molecular transport across cell membranes in response to various signals (100). Hundreds of MPs mediate both passive and active flow of ions and small molecules across membranes, contributing to complex functions such as muscle contraction, neuronal signaling and metabolism (101). Transport mechanisms vary among MP classes based on driving force, molecular selectivity, and time scale. For example, transmembrane channels are passive pores that move specific molecules down energetically favorable concentration gradients at high rates (up to 10^8 molecules per second), while transporters operate on longer timescales as they go through conformational changes to transport solutes up or down their concentration gradients (102). Pumps, on the other hand, are defined as those MPs

capable of transporting ions and other molecules against concentration gradients using energy provided from ATP hydrolysis or light (103).

Chlorophyll-based technologies have drawn increasing interest given that natural photosynthetic processes convert solar energy at rates that far exceed current global energy demands (104). Chlorophyll a/b, the major photosynthetic pigments found in green plants, are noncovalently bound to a MP that makes up two-thirds of the molecular mass of the light-harvesting chlorophyll a/b complex (LHCII). LCHII has been exploited as a biomimetic light-harvesting component in energy systems with efforts directed at expanding its absorption range, integrating it with type II quantum dots for efficient energy transfer, and using it as a photosensitizer (105-107). However, protein denaturation and pigment dissociation at high temperatures have hampered the development of these technologies (108). Based on the observations that entrapment in silica sol-gel networks can stabilize enzymes, but that autocatalytic polycondensation of silicic acid can damage them (109), Roeder and coworkers fused the R5 peptide to the N-terminus of LCHII to precipitate amorphous silica around the complex (108, 110, 111). The entrapped LHCII remained functional at 50°C for up to 24 h instead of a few minutes when stabilized by detergents. To tackle the issue of incomplete coverage of the solar spectrum, Liu and coworkers combined *Arabidopsis thaliana* LHCII, which absorbs light within most of the visible spectrum, with the *Rhodobacter sphaeroides* bacteriochlorophyll-based photochemical reaction center (RC) which covers parts of the near-UV and near-IR (**Figure 4A-C**) (104). Both proteins were modified with C-terminal decahistidine (His_{10}) extensions that allowed them to bind to CdTe quantum dots. The resulting architecture enabled much more efficient energy transfer compared to natural photosystems.

Beyond light-harvesting materials, the precision and efficiency of MP-based transport has been exploited to create bionanoelectronic devices that convert biochemical gradients into signals that can be read or processed by conventional electronics (112, 113). By integrating the Gramicidin A and Alamethicin ion channels within a supported lipid bilayer (SLB) interfaced with a palladium contact in a microfluidic device, Hemmatian *et al.* demonstrated a novel bioprotonic device capable of translating protonic (H^+) currents into electronic signals (101). The working principle is the formation of palladium hydride (PdHx) when protons that have been transported across the SLB diffuse to the Pd surface and are reduced by incoming electrons. To develop a light-controlled version of the device, *H. turkmenica* deltarhodopsin (HtdR), a green light-activated outwards proton pump, was modified with a N-terminal palladium-binding peptide (Pd4; TSNAVHPTLRHL) that was embedded within the SLB (**Figure 4D-G**) (113). When proton pumping was initiated across the bilayer by exposing the device to 523 nm light, an electric current that responded to the "on" and "off" states of illumination was observed within seconds, compared to about 1 min for a bacteriorhodopsin-based silicon nanowire device described by Noy and coworkers (114, 115). Importantly, the presence of the Pd4 extension was critical for the development of an appreciable photocurrent, presumably because it reduces the proton diffusion path length by helping HtdR form a close contact with the Pd interface. In subsequent work, a blue-absorbing proteorhodopsin (BPR) from marine bacteria was similarly fitted with a N-terminal Pd4 extension (116). Devices built with Pd4-HtdR and Pd4-BPR developed peak photocurrents when illuminated at wavelengths corresponding to the absorption maxima of the embedded rhodopsins. This enabled the detection of discrete wavelengths of light over the 450-600 nm range by measuring the associated photocurrents, opening the door to the creation of biological cameras.

5. CONCLUSIONS AND OUTLOOK

From biomineralization to organization at the nanoscale, and from catalysis to device fabrication, the above examples illustrate the broad range of technological advances that solid binding proteins have enabled over the past decade. However, the vast universe of structures and functions that natural proteins offer remains largely untapped, as do recent progress in *de novo* protein design that have enabled the creation of 1D filaments and rods (117, 118), 2D arrays (119, 120), and 3D cages (121, 122). Coupling these frameworks with one or more SBPs holds exceptional promise for the design of new classes of hybrid and hierarchical materials whose atomically precise features will give rise to new functionalities and allow for more effective control of composition, morphology and crystallography in biomineralization schemes. It is also worth noting that all solid-binding proteins built to date have exploited a very limited number of SBPs (e.g., polyhistidine extensions, R5, mTBP, Pd4, Ag4, GBP, Car9...) and that little attention has been paid to the potential of post-translational modifications for augmenting or tailoring SBP function. Making use of an expanded SBP sequence space could enable new capabilities. Indeed, when Voigt and colleagues equipped *E. coli* with heterologous enzymatic pathways to modify the R5 peptide post-translationally, they found that phosphorylation, methylation, acetylation and myristoylation (addition of an aliphatic chain) all impacted the size and/or morphology of silica particles precipitated by the peptide (123).

As tight integration of simulations and experiments fuels our understanding of how SBP sequence, structure, and self-association - and the chemical and structural context these peptides experience when part of solid-binding proteins - influence adhesion and precipitation behavior, it will be important to recall that solution conditions and interfaces also play critical roles in adhesion and

mineralization. Targeted exploration of this space guided by simulation and theory, together with the use of algorithmic and high-throughput approaches, and the consideration of far from equilibrium conditions should lead to the formulation of more holistic (and robust) rules for predictive materials design (124-127). We anticipate that these lines of research will open the door to the fabrication of sophisticated hybrid and hierarchical systems whose structure, composition and properties can be shifted on the fly to best respond to a practical need. We also expect that they will usher in a few emergent behavior surprises.

ACKNOWLEDGMENT

This material is based upon work supported by the US Department of Energy, Office of Science, Office of Basic Energy Sciences, as part of the Energy Frontier Research Centers program: CSSAS, The Center for the Science of Synthesis Across Scales under Award Number DE-SC0019288. NYN gratefully acknowledges support from a Clean Energy Institute Fellowship.

Figures

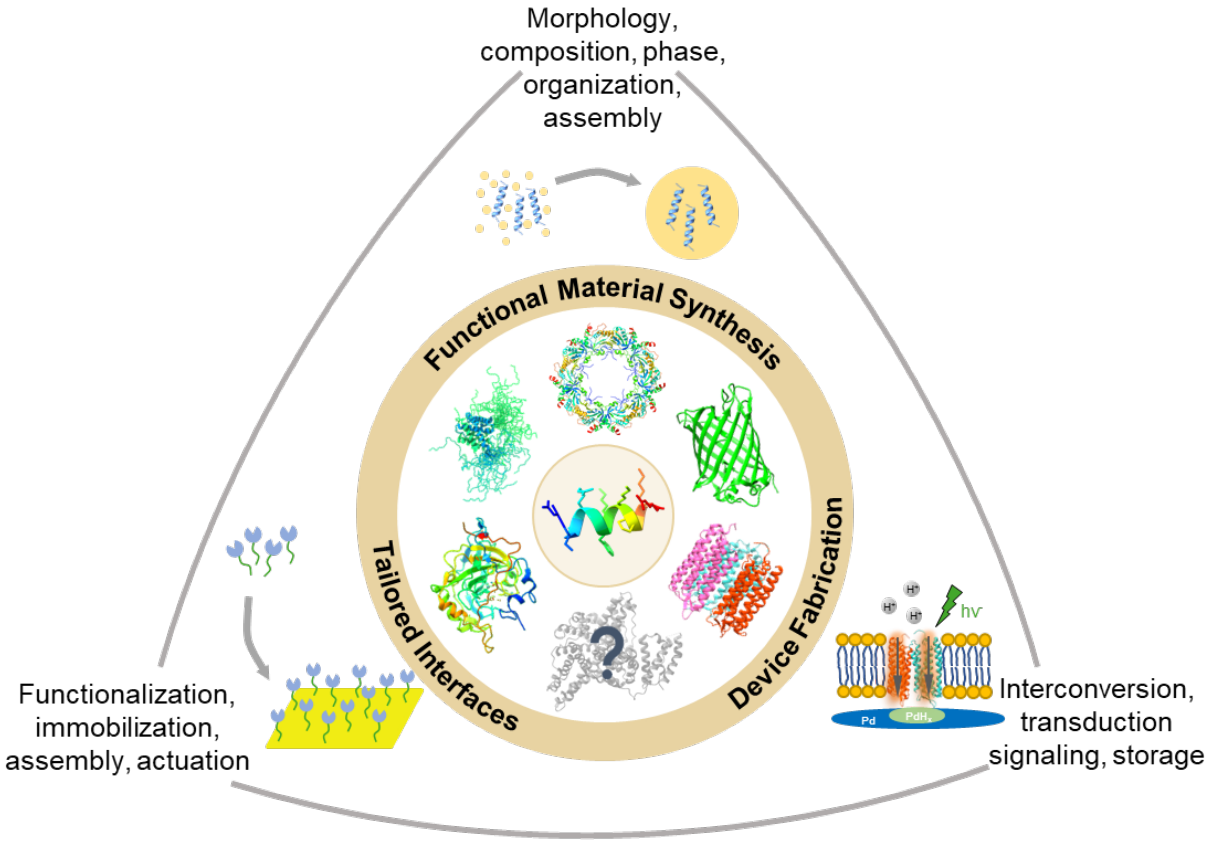

Figure 1. Schematic illustration of various protein scaffolds (middle ring) that have served as hosts for solid-binding peptides (center) and application spaces of the resulting solid-binding proteins (outer ring).

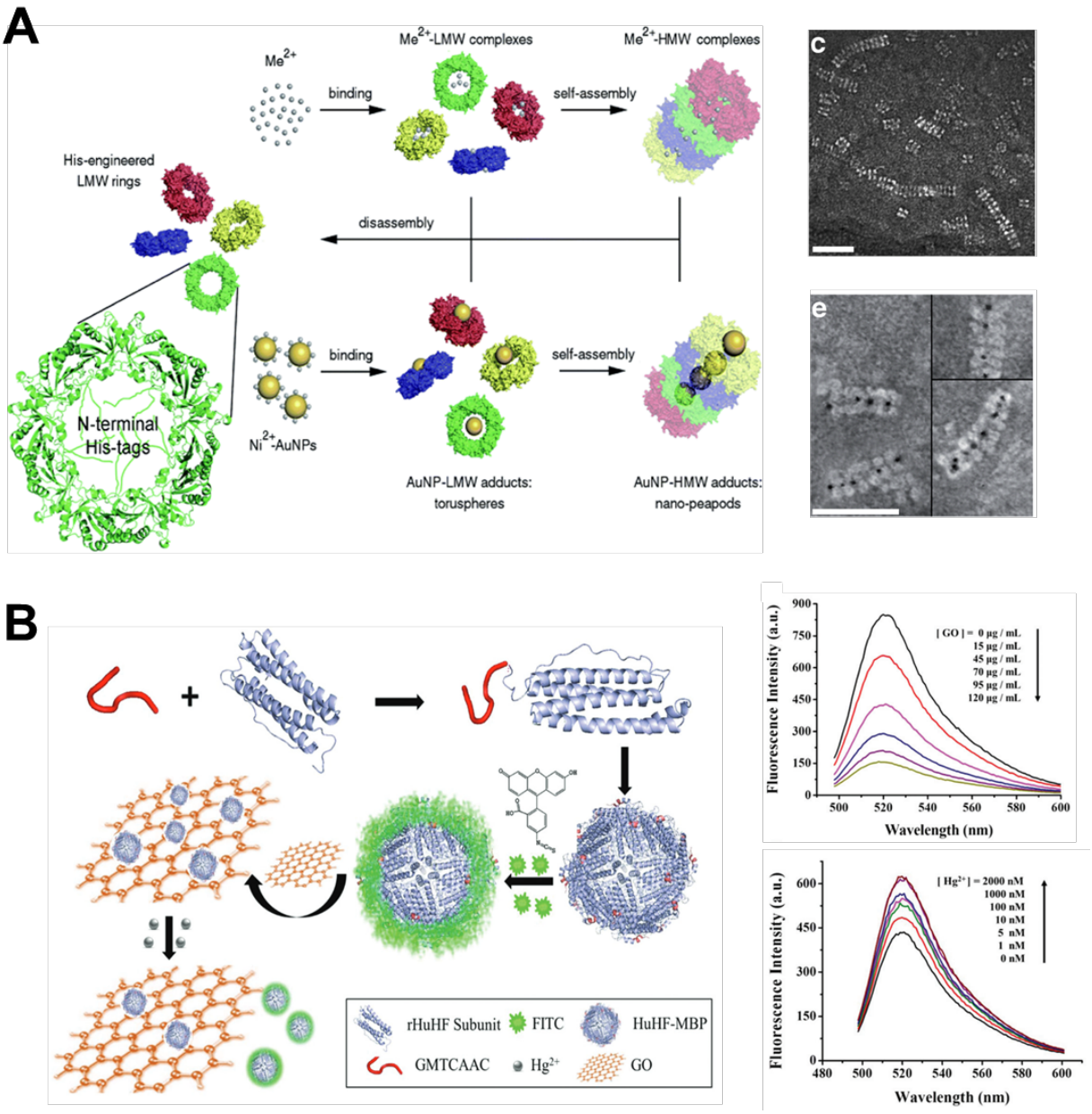

Figure 2. Applications of solid-binding ring and shell proteins. **(A)** Schematic illustration and TEM images of 6His-SmPrxI self-assembly upon addition of divalent metal ions (top) or Ni^{2+}-NTA-coated gold nanoparticles (bottom). **(B)** Schematic illustration of a ferritin-based platform for Hg^{2+} detection. Mercury-binding peptides (red) displayed on the exterior surface of the ferritin nanocage are further derivatized with FITC (green) whose fluorescence is quenched by graphene oxide (orange) but recovered upon addition of Hg^{2+} (silver). Fluorescence emission spectra on the right shows the concentration-dependent quenching of FITC fluorescence with GO, and the dose-dependent recovery of fluorescence recovery upon addition of Hg^{2+} ions. Adapted with permission from references 74 and 83.

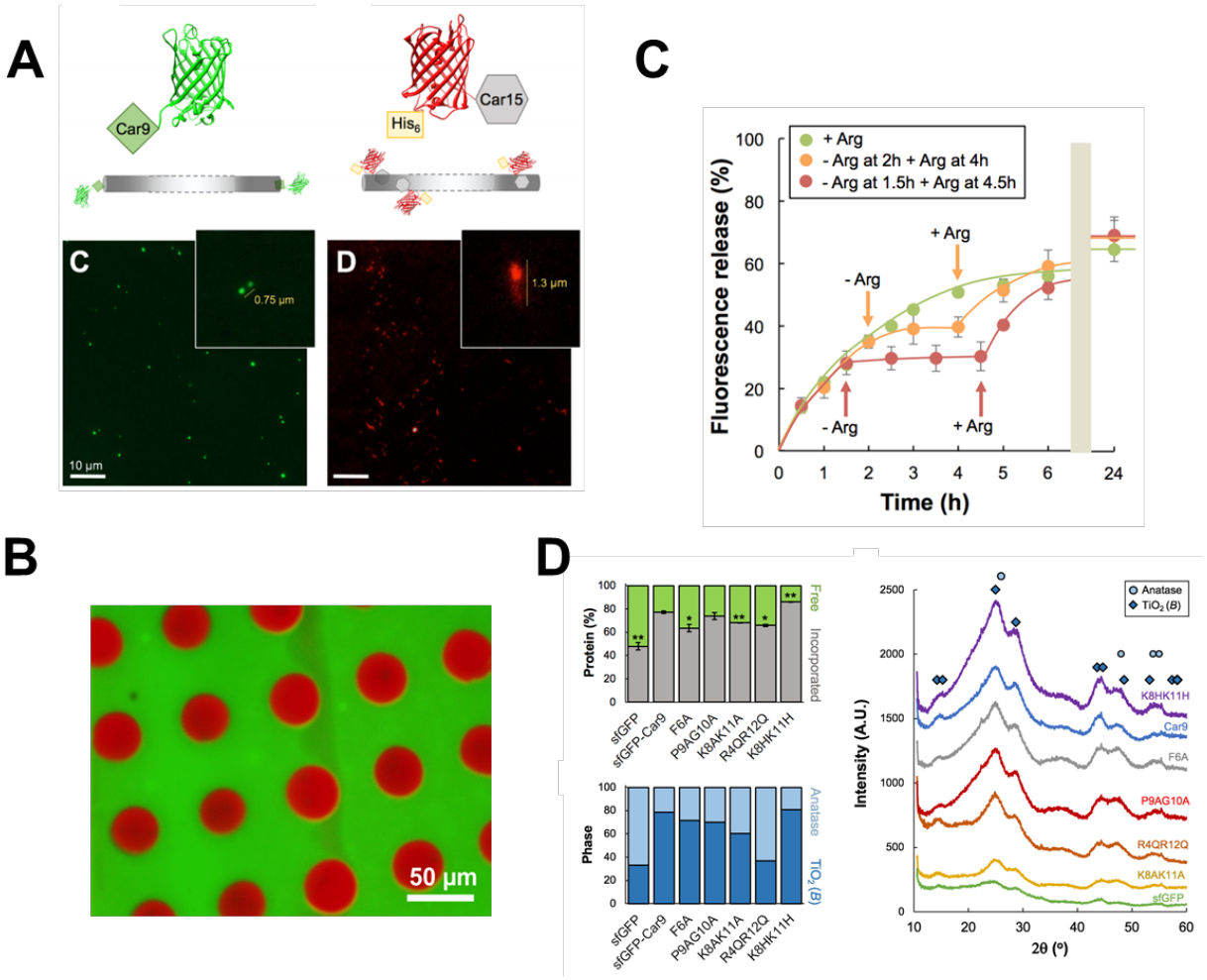

Figure 3. Applications of solid-binding fluorescent proteins. (**A**) Visualization of the selective labelling of the ends and sidewalls of single-walled carbon nanotubes by Car9 and Car15 derivatives of sfGFP and mCherry. (**B**) Fabrication of a bicontinuous protein pattern on microscope slides via microcontact printing of sfGFP-Car9 (green field) and backfilling of bare areas with mCherry-Car9. (**C**) Continuous and discontinuous release of sfGFP-Car9 self-immobilized within the porous network produced during the formation of silica sol-gels. Incubation of the protein-loaded sol-gel in arginine-containing buffer triggers protein release but the process can be stopped by washing the particles in buffer and reinitiated at a later time by addition of arginine. (**D**) Titania precipitated from acidified solutions of TiBALDH using sfGFP-Car9 or variants containing substitutions in the SBP segment is mainly amorphous but contains anatase and TiO_2(B) (i.e., monoclinic) nanocrystalline inclusions whose relative abundance can be tuned by the choice of mutation. Adapted with permission from references 92, 95, 96 and 98.

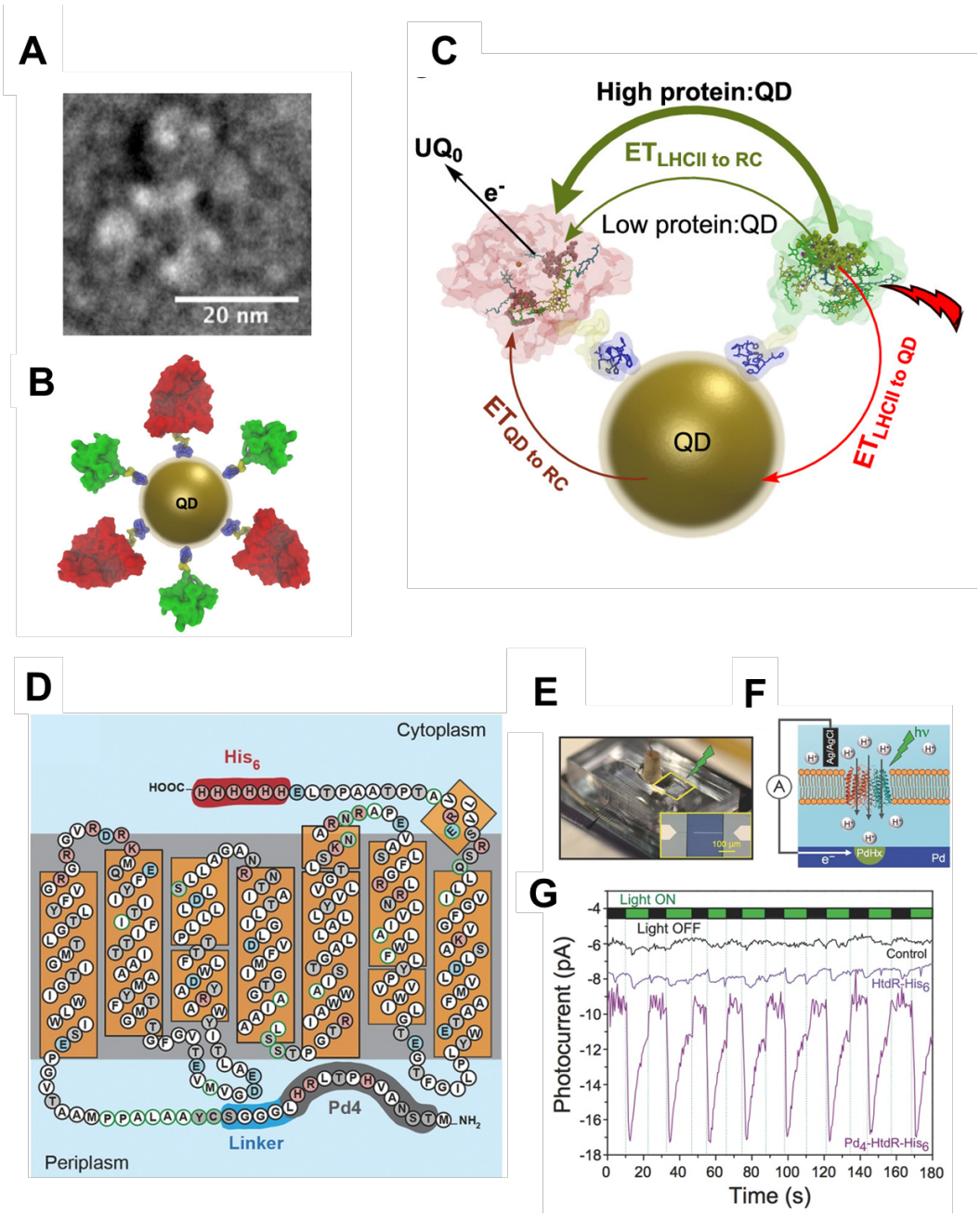

Figure 4. Applications of light-activated solid-binding proteins. (**A**) Transmission electron micrograph of an individual LHCIIH/RCH/QD tricomponent nanoconjugate. (**B**) Schematic representation of an LHCIIH/RCH/QD nanoconjugate with LHCIIH shown in green, RCH in red, flexible linkers in yellow, and the His-tag in blue. (**C**) Schematic of an LHCIIH/RCH/QD nanoconjugate with routes of direct and indirect FRET. (**D**) Predicted topology of Pd4-HtdR-His$_6$ in the inner membrane of *E. coli*. Picture (**E**) and schematic (**F**) of the bioprotonic device. (**G**) Photocurrent response of the device prepared with control liposomes (black trace), HtdR-His$_6$ (blue) or Pd4-HtdR-His6 proteoliposomes (purple) exposed to successive 10 s illumination cycles with a 523 nm LED. Adapted with permission from references 104 and 113.

1. Wang C-y, Jiao K, Yan J-f, Wan M-c, Wan Q-q, et al. 2020. Biological and synthetic template-directed syntheses of mineralized hybrid and inorganic materials. *Prog. Mater Sci.*: 100712
2. Liu X, Zhang F, Jing X, Pan M, Liu P, et al. 2018. Complex silica composite nanomaterials templated with DNA origami. *Nature* 559: 593-98
3. Ramakrishnan S, Ijäs H, Linko V, Keller A. 2018. Structural stability of DNA origami nanostructures under application-specific conditions. *Comput. Struct. Biotechnol. J.* 16: 342-49
4. Jin H, Qiu H, Sakamoto Y, Shu P, Terasaki O, Che S. 2008. Mesoporous Silicas by Self-Assembly of Lipid Molecules: Ribbon, Hollow Sphere, and Chiral Materials. *CEJ* 14: 6413-20
5. S M Gruner, P R Cullis, M J Hope a, Tilcock CPS. 1985. Lipid Polymorphism:The Molecular Basis of Nonbilayer Phases. *Annu. Rev. Biophys* 14: 211-38
6. Battigelli A. 2019. Design and preparation of organic nanomaterials using self-assembled peptoids. *Biopolymers* 110: e23265
7. Robertson EJ, Battigelli A, Proulx C, Mannige RV, Haxton TK, et al. 2016. Design, Synthesis, Assembly, and Engineering of Peptoid Nanosheets. *Acc. Chem. Res.* 49: 379-89
8. Liu CC, Schultz PG. 2010. Adding New Chemistries to the Genetic Code. *Annu. Rev. Biochem.* 79: 413-44
9. Baker D. 2019. What has de novo protein design taught us about protein folding and biophysics? *Protein Sci.* 28: 678-83
10. Torculas M, Medina J, Xue W, Hu X. 2016. Protein-Based Bioelectronics. *ACS Biomater. Sci. Eng.* 2: 1211-23
11. Brokesh AM, Gaharwar AK. 2020. Inorganic Biomaterials for Regenerative Medicine. *ACS Appl. Mater. Interfaces* 12: 5319-44
12. Zeymer C, Hilvert D. 2018. Directed Evolution of Protein Catalysts. *Annu. Rev. Biochem.* 87: 131-57
13. Dickerson MB, Sandhage KH, Naik RR. 2008. Protein- and Peptide-Directed Syntheses of Inorganic Materials. *Chem. Rev.* 108: 4935-78
14. Brown S. 1997. Metal-recognition by repeating polypeptides. *Nat. Biotechnol.* 15: 269-72
15. Rehm B. 2013. *Bionanotechnology: Biological Self-assembly and Its Applications*: Caister Academic Press
16. Newton MS, Cabezas-Perusse Y, Tong CL, Seelig B. 2020. In Vitro Selection of Peptides and Proteins—Advantages of mRNA Display. *ACS Synth. Biol.* 9: 181-90
17. Plückthun A. 2012. Ribosome Display: A Perspective. In *Ribosome Display and Related Technologies: Methods and Protocols*, ed. JA Douthwaite, RH Jackson, pp. 3-28. New York, NY: Springer New York
18. Smith GP, Petrenko VA. 1997. Phage Display. *Chem. Rev.* 97: 391-410
19. Fang Y, Poulsen N, Dickerson MB, Cai Y, Jones SE, et al. 2008. Identification of peptides capable of inducing the formation of titania but not silica via a subtractive bacteriophage display approach. *J. Mater. Chem.* 18: 3871-75
20. Juds C, Schmidt J, Weller MG, Lange T, Beck U, et al. 2020. Combining Phage Display and Next-Generation Sequencing for Materials Sciences: A Case Study on Probing Polypropylene Surfaces. *J. Am. Chem. Soc.* 142: 10624-28
21. Bansal R, Care A, Lord MS, Walsh TR, Sunna A. 2019. Experimental and theoretical tools to elucidate the binding mechanisms of solid-binding peptides. *N. Biotechnol.* 52: 9-18
22. Bhimanapati GR, Lin Z, Meunier V, Jung Y, Cha J, et al. 2015. Recent Advances in Two-Dimensional Materials beyond Graphene. *ACS Nano* 9: 11509-39
23. So CR, Hayamizu Y, Yazici H, Gresswell C, Khatayevich D, et al. 2012. Controlling Self-Assembly of Engineered Peptides on Graphite by Rational Mutation. *ACS Nano* 6: 1648-56

24. Katoch J, Kim SN, Kuang Z, Farmer BL, Naik RR, et al. 2012. Structure of a Peptide Adsorbed on Graphene and Graphite. *Nano Lett.* 12: 2342-46
25. Hughes ZE, Walsh TR. 2015. What makes a good graphene-binding peptide? Adsorption of amino acids and peptides at aqueous graphene interfaces. *J Mater Chem B* 3: 3211-21
26. Zou X, Wei S, Jasensky J, Xiao M, Wang Q, et al. 2017. Molecular Interactions between Graphene and Biological Molecules. *J. Am. Chem. Soc.* 139: 1928-36
27. Wei S, Zou X, Tian J, Huang H, Guo W, Chen Z. 2019. Control of Protein Conformation and Orientation on Graphene. *J. Am. Chem. Soc.* 141: 20335-43
28. Brljak N, Parab AD, Rao R, Slocik JM, Naik RR, et al. 2020. Material composition and peptide sequence affects biomolecule affinity to and selectivity for h-boron nitride and graphene. *Chem. Commun.* 56: 8834-37
29. Chen J, Zhu E, Liu J, Zhang S, Lin Z, et al. 2018. Building two-dimensional materials one row at a time: Avoiding the nucleation barrier. *Science* 362: 1135-39
30. Hnilova M, Oren EE, Seker UOS, Wilson BR, Collino S, et al. 2008. Effect of Molecular Conformations on the Adsorption Behavior of Gold-Binding Peptides. *Langmuir* 24: 12440-45
31. Seker UOS, Wilson B, Kulp JL, Evans JS, Tamerler C, Sarikaya M. 2014. Thermodynamics of Engineered Gold Binding Peptides: Establishing the Structure–Activity Relationships. *Biomacromolecules* 15: 2369-77
32. Verde AV, Acres JM, Maranas JK. 2009. Investigating the Specificity of Peptide Adsorption on Gold Using Molecular Dynamics Simulations. *Biomacromolecules* 10: 2118-28
33. Kacar T, Zin MT, So C, Wilson B, Ma H, et al. 2009. Directed self-immobilization of alkaline phosphatase on micro-patterned substrates via genetically fused metal-binding peptide. *Biotechnol. Bioeng.* 103: 696-705
34. Wright LB, Palafox-Hernandez JP, Rodger PM, Corni S, Walsh TR. 2015. Facet selectivity in gold binding peptides: exploiting interfacial water structure. *Chem. Sci.* 6: 5204-14
35. Pacardo DB, Sethi M, Jones SE, Naik RR, Knecht MR. 2009. Biomimetic Synthesis of Pd Nanocatalysts for the Stille Coupling Reaction. *ACS Nano* 3: 1288-96
36. Hughes ZE, Nguyen MA, Li Y, Swihart MT, Walsh TR, Knecht MR. 2017. Elucidating the influence of materials-binding peptide sequence on Au surface interactions and colloidal stability of Au nanoparticles. *Nanoscale* 9: 421-32
37. Nergiz SZ, Slocik JM, Naik RR, Singamaneni S. 2013. Surface defect sites facilitate fibrillation: an insight into adsorption of gold-binding peptides on Au(111). *PCCP* 15: 11629-33
38. Palafox-Hernandez JP, Tang Z, Hughes ZE, Li Y, Swihart MT, et al. 2014. Comparative Study of Materials-Binding Peptide Interactions with Gold and Silver Surfaces and Nanostructures: A Thermodynamic Basis for Biological Selectivity of Inorganic Materials. *Chem. Mater.* 26: 4960-69
39. Poblete H, Agarwal A, Thomas SS, Bohne C, Ravichandran R, et al. 2016. New Insights into Peptide–Silver Nanoparticle Interaction: Deciphering the Role of Cysteine and Lysine in the Peptide Sequence. *Langmuir* 32: 265-73
40. Aliaga AE, Ahumada H, Sepúlveda K, Gomez-Jeria JS, Garrido C, et al. 2011. SERS, Molecular Dynamics and Molecular Orbital Studies of the MRKDV Peptide on Silver and Membrane Surfaces. *J. Phys. Chem. C* 115: 3982-89
41. Patwardhan SV, Emami FS, Berry RJ, Jones SE, Naik RR, et al. 2012. Chemistry of Aqueous Silica Nanoparticle Surfaces and the Mechanism of Selective Peptide Adsorption. *J. Am. Chem. Soc.* 134: 6244-56
42. Puddu V, Perry CC. 2012. Peptide Adsorption on Silica Nanoparticles: Evidence of Hydrophobic Interactions. *ACS Nano* 6: 6356-63
43. Puddu V, Perry CC. 2014. Interactions at the Silica–Peptide Interface: The Influence of Particle Size and Surface Functionality. *Langmuir* 30: 227-33

44. Sola-Rabada A, Michaelis M, Oliver DJ, Roe MJ, Colombi Ciacchi L, et al. 2018. Interactions at the Silica–Peptide Interface: Influence of the Extent of Functionalization on the Conformational Ensemble. *Langmuir* 34: 8255-63
45. Hellner B, Lee SB, Subramaniam A, Subramanian VR, Baneyx F. 2019. Modeling the Cooperative Adsorption of Solid-Binding Proteins on Silica: Molecular Insights from Surface Plasmon Resonance Measurements. *Langmuir* 35: 5013-20
46. Hellner B, Alamdari S, Pyles H, Zhang S, Prakash A, et al. 2020. Sequence–Structure–Binding Relationships Reveal Adhesion Behavior of the Car9 Solid-Binding Peptide: An Integrated Experimental and Simulation Study. *J. Am. Chem. Soc.* 142: 2355-63
47. Chen H, Su X, Neoh K-G, Choe W-S. 2009. Context-Dependent Adsorption Behavior of Cyclic and Linear Peptides on Metal Oxide Surfaces. *Langmuir* 25: 1588-93
48. Sultan AM, Westcott ZC, Hughes ZE, Palafox-Hernandez JP, Giesa T, et al. 2016. Aqueous Peptide–TiO2 Interfaces: Isoenergetic Binding via Either Entropically or Enthalpically Driven Mechanisms. *ACS Appl. Mater. Interfaces* 8: 18620-30
49. Sano K-I, Shiba K. 2003. A Hexapeptide Motif that Electrostatically Binds to the Surface of Titanium. *J. Am. Chem. Soc.* 125: 14234-35
50. Suzuki Y, Shindo H, Asakura T. 2016. Structure and Dynamic Properties of a Ti-Binding Peptide Bound to TiO2 Nanoparticles As Accessed by 1H NMR Spectroscopy. *J. Phys. Chem. B* 120: 4600-07
51. Skelton AA, Liang T, Walsh TR. 2009. Interplay of Sequence, Conformation, and Binding at the Peptide−Titania Interface as Mediated by Water. *ACS Appl. Mater. Interfaces* 1: 1482-91
52. Wu C, Skelton AA, Chen M, Vlček L, Cummings PT. 2012. Modeling the Interaction between Integrin-Binding Peptide (RGD) and Rutile Surface: The Effect of Cation Mediation on Asp Adsorption. *Langmuir* 28: 2799-811
53. Lee D, Redfern O, Orengo C. 2007. Predicting protein function from sequence and structure. *Nat. Rev. Mol. Cell Biol.* 8: 995-1005
54. Childers MC, Daggett V. 2017. Insights from molecular dynamics simulations for computational protein design. *Mol. Syst. Des. Eng.* 2: 9-33
55. Matsuurua K. 2014. Rational design of self-assembled proteins and peptides for nano- and micro-sized architectures. *RSC Adv.* 4: 2942-53
56. Huang P-S, Boyken SE, Baker D. 2016. The coming of age of de novo protein design. *Nature* 537: 320-27
57. Gainza-Cirauqui P, Correia BE. 2018. Computational protein design—the next generation tool to expand synthetic biology applications. *Curr. Opin. Biotechnol.* 52: 145-52
58. Tompa P. 2012. Intrinsically disordered proteins: a 10-year recap. *Trends Biochem. Sci.* 37: 509-16
59. Huang H-C, Nanda A, Rege K. 2012. Investigation of Phase Separation Behavior and Formation of Plasmonic Nanocomposites from Polypeptide-Gold Nanorod Nanoassemblies. *Langmuir* 28: 6645-55
60. Han W, MacEwan SR, Chilkoti A, López GP. 2015. Bio-inspired synthesis of hybrid silica nanoparticles templated from elastin-like polypeptide micelles. *Nanoscale* 7: 12038-44
61. Li L, Li NK, Tu Q, Im O, Mo C-K, et al. 2018. Functional Modification of Silica through Enhanced Adsorption of Elastin-Like Polypeptide Block Copolymers. *Biomacromolecules* 19: 298-306
62. Teulé F, Cooper AR, Furin WA, Bittencourt D, Rech EL, et al. 2009. A protocol for the production of recombinant spider silk-like proteins for artificial fiber spinning. *Nat. Protoc.* 4: 341-55
63. Plowright R, Dinjaski N, Zhou S, Belton DJ, Kaplan DL, Perry CC. 2016. Influence of silk–silica fusion protein design on silica condensation in vitro and cellular calcification. *RSC Adv.* 6: 21776-88

64. Currie HA, Deschaume O, Naik RR, Perry CC, Kaplan DL. 2011. Genetically engineered chimeric silk-silver binding proteins. *Adv. Funct. Mater.* 21: 2889-95
65. Henderson CJ, Pumford E, Seevaratnam DJ, Daly R, Hall EAH. 2019. Gene to diagnostic: Self immobilizing protein for silica microparticle biosensor, modelled with sarcosine oxidase. *Biomaterials* 193: 58-70
66. Yang M, Choi BG, Park TJ, Heo NS, Hong WH, Lee SY. 2011. Site-specific immobilization of gold binding polypeptide on gold nanoparticle-coated graphene sheet for biosensor application. *Nanoscale* 3: 2950-56
67. Savile CK, Lalonde JJ. 2011. Biotechnology for the acceleration of carbon dioxide capture and sequestration. *Curr. Opin. Biotechnol.* 22: 818-23
68. Kim S, Joo KI, Jo BH, Cha HJ. 2020. Stability-Controllable Self-Immobilization of Carbonic Anhydrase Fused with a Silica-Binding Tag onto Diatom Biosilica for Enzymatic CO2 Capture and Utilization. *ACS Appl. Mater. Interfaces* 12: 27055-63
69. Kim JK, Abdelhamid MAA, Pack SP. 2019. Direct immobilization and recovery of recombinant proteins from cell lysates by using EctP1-peptide as a short fusion tag for silica and titania supports. *Int. J. Biol. Macromol.* 135: 969-77
70. Butz ZJ, Borgognoni K, Nemeth R, Nilsson ZN, Ackerson CJ. 2020. Metalloid Reductase Activity Modified by a Fused Se0 Binding Peptide. *ACS Chem. Biol.* 15: 1987-95
71. Care A, Petroll K, Gibson ESY, Bergquist PL, Sunna A. 2017. Solid-binding peptides for immobilisation of thermostable enzymes to hydrolyse biomass polysaccharides. *Biotechnol. Biofuels* 10: 29
72. McMillan RA, Paavola CD, Howard J, Chan SL, Zaluzec NJ, Trent JD. 2002. Ordered nanoparticle arrays formed on engineered chaperonin protein templates. *Nat. Mater.* 1: 247-52
73. Ishii D, Kinbara K, Ishida Y, Ishii N, Okochi M, et al. 2003. Chaperonin-mediated stabilization and ATP-triggered release of semiconductor nanoparticles. *Nature* 423: 628-32
74. Ardini M, Giansanti F, Di Leandro L, Pitari G, Cimini A, et al. 2014. Metal-induced self-assembly of peroxiredoxin as a tool for sorting ultrasmall gold nanoparticles into one-dimensional clusters. *Nanoscale* 6: 8052-61
75. Ardini M, Golia G, Passaretti P, Cimini A, Pitari G, et al. 2016. Supramolecular self-assembly of graphene oxide and metal nanoparticles into stacked multilayers by means of a multitasking protein ring. *Nanoscale* 8: 6739-53
76. Domigan LJ, Ashmead H, Dimartino S, Malmstrom J, Pearce FG, et al. 2017. Formation of supramolecular protein structures on gold surfaces. *Biointerphases* 12: 04E405
77. Schreiber A, Huber MC, Cölfen H, Schiller SM. 2015. Molecular protein adaptor with genetically encoded interaction sites guiding the hierarchical assembly of plasmonically active nanoparticle architectures. *Nat. Commun* 6: 6705
78. Heyman A, Medalsy I, Bet Or O, Dgany O, Gottlieb M, et al. 2009. Protein Scaffold Engineering Towards Tunable Surface Attachment. *Angew. Chem.* 48: 9290-94
79. Bachar O, Meirovich MM, Kurzion R, Yehezkeli O. 2020. In vivo and in vitro protein mediated synthesis of palladium nanoparticles for hydrogenation reactions. *Chem. Commun.* 56: 11211-14
80. Massover WH. 1993. Ultrastructure of ferritin and apoferritin: A review. *Micron* 24: 389-437
81. Zheng B, Yamashita I, Uenuma M, Iwahori K, Kobayashi M, Uraoka Y. 2009. Site-directed delivery of ferritin-encapsulated gold nanoparticles. *Nanotechnology* 21: 045305
82. Nguyen TKM, Ki MR, Lee CS, Pack SP. 2019. Nanosized and tunable design of biosilica particles using novel silica-forming peptide-modified chimeric ferritin templates. *J Ind Eng Chem* 73: 198-204
83. Wang Y, Chen H, Zang J, Zhang X, Zhao G. 2019. Re-designing ferritin nanocages for mercuric ion detection. *Analyst* 144: 5890-97

84. Pieters BJGE, van Eldijk MB, Nolte RJM, Mecinović J. 2016. Natural supramolecular protein assemblies. *Chem. Soc. Rev.* 45: 24-39
85. Zimmer M. 2002. Green Fluorescent Protein (GFP): Applications, Structure, and Related Photophysical Behavior. *Chem. Rev.* 102: 759-82
86. Pédelacq J-D, Cabantous S, Tran T, Terwilliger TC, Waldo GS. 2006. Engineering and characterization of a superfolder green fluorescent protein. *Nat. Biotechnol.* 24: 79-88
87. Zhang G, Gurtu V, Kain SR. 1996. An Enhanced Green Fluorescent Protein Allows Sensitive Detection of Gene Transfer in Mammalian Cells. *Biochem. Biophys. Res. Commun.* 227: 707-11
88. Chudakov DM, Matz MV, Lukyanov S, Lukyanov KA. 2010. Fluorescent Proteins and Their Applications in Imaging Living Cells and Tissues. *Physiol. Rev.* 90: 1103-63
89. Soundrarajan N, Cho H-s, Ahn B, Choi M, Thong LM, et al. 2016. Green fluorescent protein as a scaffold for high efficiency production of functional bacteriotoxic proteins in Escherichia coli. *Sci. Rep.* 6: 20661
90. Hnilova M, Liu X, Yuca E, Jia C, Wilson B, et al. 2012. Multifunctional Protein-Enabled Patterning on Arrayed Ferroelectric Materials. *ACS Appl. Mater. Interfaces* 4: 1865-71
91. Coyle BL, Rolandi M, Baneyx F. 2013. Carbon-Binding Designer Proteins that Discriminate between sp2- and sp3-Hybridized Carbon Surfaces. *Langmuir* 29: 4839-46
92. Dunakey SJG, Coyle BL, Thomas A, Xu M, Swift BJF, Baneyx F. 2019. Selective Labeling and Decoration of the Ends and Sidewalls of Single-Walled Carbon Nanotubes Using Mono- and Bispecific Solid-Binding Fluorescent Proteins. *Bioconj. Chem.* 30: 959-65
93. Coyle BL, Baneyx F. 2014. A cleavable silica-binding affinity tag for rapid and inexpensive protein purification. 111: 2019-26
94. Xu M, Bailey MJ, Look J, Baneyx F. 2020. Affinity purification of Car9-tagged proteins on silica-derivatized spin columns and 96-well plates. *Protein Expr. Purif.* 170: 105608
95. Coyle BL, Baneyx F. 2016. Direct and reversible immobilization and microcontact printing of functional proteins on glass using a genetically appended silica-binding tag. *Chem. Commun.* 52: 7001-04
96. Yang W, Hellner B, Baneyx F. 2016. Self-Immobilization of Car9 Fusion Proteins within High Surface Area Silica Sol–Gels and Dynamic Control of Protein Release. *Bioconj. Chem.* 27: 2450-59
97. Olmez TT, Yuca E, Eyupoglu E, Catalak HB, Sahin O, Seker UOS. 2018. Autonomous Synthesis of Fluorescent Silica Biodots Using Engineered Fusion Proteins. *ACS Omega* 3: 585-94
98. Hellner B, Stegmann AE, Pushpavanam K, Bailey MJ, Baneyx F. 2020. Phase Control of Nanocrystalline Inclusions in Bioprecipitated Titania with a Panel of Mutant Silica-Binding Proteins. *Langmuir* 36: 8503-10
99. Swift BJF, Shadish JA, DeForest CA, Baneyx F. 2017. Streamlined Synthesis and Assembly of a Hybrid Sensing Architecture with Solid Binding Proteins and Click Chemistry. *J. Am. Chem. Soc.* 139: 3958-61
100. Alberts B, Johnson A, Lewis J, Walter P, Raff M, Roberts K. 2002. *Molecular Biology of the Cell 4th Edition: International Student Edition*: Routledge
101. Hemmatian Z, Keene S, Josberger E, Miyake T, Arboleda C, et al. 2016. Electronic control of H+ current in a bioprotonic device with Gramicidin A and Alamethicin. *Nat. Commun* 7: 12981
102. Lodish HF. 2008. *Molecular Cell Biology 6 Ed*: W. H. Freeman and Company
103. Shen Y-x, Saboe PO, Sines IT, Erbakan M, Kumar M. 2014. Biomimetic membranes: A review. *J. Membr. Sci.* 454: 359-81
104. Liu J, Mantell J, Jones MR. 2020. Minding the Gap between Plant and Bacterial Photosynthesis within a Self-Assembling Biohybrid Photosystem. *ACS Nano* 14: 4536-49

105. Gundlach K, Werwie M, Wiegand S, Paulsen H. 2009. Filling the “green gap” of the major light-harvesting chlorophyll a/b complex by covalent attachment of Rhodamine Red. *Biochim. Biophys. Acta* 1787: 1499-504
106. Werwie M, Xu X, Haase M, Basché T, Paulsen H. 2012. Bio Serves Nano: Biological Light-Harvesting Complex as Energy Donor for Semiconductor Quantum Dots. *Langmuir* 28: 5810-18
107. Nagata M, Amano M, Joke T, Fujii K, Okuda A, et al. 2012. Immobilization and Photocurrent Activity of a Light-Harvesting Antenna Complex II, LHCII, Isolated from a Plant on Electrodes. *ACS Macro Lett.* 1: 296-99
108. Roeder S, Hobe S, Paulsen H. 2014. Silica Entrapment for Significantly Stabilized, Energy-Conducting Light-Harvesting Complex (LHCII). *Langmuir* 30: 14234-40
109. Patwardhan SV, Holt SA, Kelly SM, Kreiner M, Perry CC, van der Walle CF. 2010. Silica Condensation by a Silicatein α Homologue Involves Surface-Induced Transition to a Stable Structural Intermediate Forming a Saturated Monolayer. *Biomacromolecules* 11: 3126-35
110. O'Neill H, Greenbaum E. 2005. Spectroscopy and Photochemistry of Spinach Photosystem I Entrapped and Stabilized in a Hybrid Organosilicate Glass. *Chem. Mater.* 17: 2654-61
111. Braun S, Rappoport S, Zusman R, Avnir D, Ottolenghi M. 2007. Biochemically active sol-gel glasses: The trapping of enzymes. *Mater. Lett.* 61: 2843-46
112. Huang S-CJ, Artyukhin AB, Misra N, Martinez JA, Stroeve PA, et al. 2010. Carbon Nanotube Transistor Controlled by a Biological Ion Pump Gate. *Nano Lett.* 10: 1812-16
113. Soto-Rodríguez J, Hemmatian Z, Josberger EE, Rolandi M, Baneyx F. 2016. A Palladium-Binding Deltarhodopsin for Light-Activated Conversion of Protonic to Electronic Currents. *Adv. Mater.* 28: 6581-85
114. Misra N, Martinez JA, Huang S-CJ, Wang Y, Stroeve P, et al. 2009. Bioelectronic silicon nanowire devices using functional membrane proteins. *PNAS* 106: 13780-84
115. Tunuguntla RH, Bangar MA, Kim K, Stroeve P, Grigoropoulos C, et al. 2015. Bioelectronic Light-Gated Transistors with Biologically Tunable Performance. *Adv. Mater.* 27: 831-36
116. Soto-Rodríguez J, Hemmatian Z, Black J, Rolandi M, Baneyx F. 2019. Two-Channel Bioprotonic Photodetector. *ACS Appl. Bio Mater.* 2: 930-35
117. Pyles H, Zhang S, De Yoreo JJ, Baker D. 2019. Controlling protein assembly on inorganic crystals through designed protein interfaces. *Nature* 571: 251-56
118. Shen H, Fallas JA, Lynch E, Sheffler W, Parry B, et al. 2018. De novo design of self-assembling helical protein filaments. *Science* 362: 705-09
119. Matthaei JF, DiMaio F, Richards JJ, Pozzo LD, Baker D, Baneyx F. 2015. Designing Two-Dimensional Protein Arrays through Fusion of Multimers and Interface Mutations. *Nano Lett.* 15: 5235-39
120. Gonen S, DiMaio F, Gonen T, Baker D. 2015. Design of ordered two-dimensional arrays mediated by noncovalent protein-protein interfaces. *Science* 348: 1365-68
121. Bale JB, Gonen S, Liu Y, Sheffler W, Ellis D, et al. 2016. Accurate design of megadalton-scale two-component icosahedral protein complexes. *Science* 353: 389-94
122. Hsia Y, Bale JB, Gonen S, Shi D, Sheffler W, et al. 2016. Design of a hyperstable 60-subunit protein dodecahedron. *Nature* 535: 136-39
123. Wallace AK, Chanut N, Voigt CA. 2020. Silica Nanostructures Produced Using Diatom Peptides with Designed Post-Translational Modifications. *Adv. Funct. Mater.* 30: 2000849
124. Nakouzi E, Steinbock O. 2016. Self-organization in precipitation reactions far from the equilibrium. *Sci. Adv.* 2: e1601144
125. Sampath J, Alamdari S, Pfaendtner J. 2020. Closing the Gap Between Modeling and Experiments in the Self-Assembly of Biomolecules at Interfaces and in Solution. *Chem. Mater.* 32: 8043-59

126. Basith S, Manavalan B, Hwan Shin T, Lee G. 2020. Machine intelligence in peptide therapeutics: A next-generation tool for rapid disease screening. *Med. Res. Rev.* 40: 1276-314
127. Vinogradov AA, Gates ZP, Zhang C, Quartararo AJ, Halloran KH, Pentelute BL. 2017. Library Design-Facilitated High-Throughput Sequencing of Synthetic Peptide Libraries. *ACS Comb. Sci.* 19: 694-701